High spatial resolution analysis of ferromanganese concretions by LA-ICP-MS†

Mikael D. Axelsson,*[a] Ilia Rodushkin,[b] Douglas C. Baxter,[c] Johan Ingri[a] and Björn Öhlander[a]

[a]*Division of Applied Geology, Luleå University of Technology, SE-971 87 Luleå, Sweden*
[b]*SGAB Analytica, Luleå University of Technology, SE-971 87 Luleå, Sweden*
[c]*Division of Inorganic Chemistry, Luleå University of Technology, SE-971 87 Luleå, Sweden*

Article

Received 2nd May 2002, Accepted 5th June 2002
Published on the Web 13th June 2002

A procedure was developed for the determination of element distributions in cross-sections of ferromanganese concretions using laser ablation inductively coupled plasma mass spectrometry (LA-ICP-MS). The effects of carrier flow rates, rf forward power, ablation energy, ablation spot size, repetition rate and number of shots per point on analyte intensity were studied. It is shown that different carrier gas flow rates are required in order to obtain maximum sensitivities for different groups of elements, thus complicating the optimisation of ICP parameters. On the contrary, LA parameters have very similar effects on almost all elements studied, thus providing a common optimum parameter set for the entire mass range. However, for selected LA parameters, the use of compromise conditions was necessary in order to compensate for relatively slow data acquisition by ICP-MS and maintain high spatial resolution without sacrificing the multielemental capabilities of the technique. Possible variations in ablation efficiency were corrected for mathematically using the sum of Fe and Mn intensities. Quantification by external calibration against matrix-matched standards was successfully used for more than 50 elements. These standards, in the form of pressed pellets (no binder), were prepared in-house using ferromanganese concentrates from a deep-sea nodule reference material as well as from shallow-marine concretions varying in size and having different proportions of three major phases: aluminosilicates, Fe- and Mn-oxyhydroxides. Element concentrations in each standard were determined by means of conventional solution nebulisation ICP-MS following acid digestion. Examples of selected inter-element correlations in distribution patterns along the cross-section of a concretion are given.

Introduction

Ferromanganese concretions are sedimentary deposits found in freshwater lakes, mires, in shallow marine and deep-sea environments. They have a complex internal layered structure primarily composed of Fe- and Mn-oxyhydroxides layers. In the early 1960s, Cameron[1] and Arrhenius[2] showed the complexity of the layering by means of photomicrographs, Burns and Fuerstenau[3] later being among the first to demonstrate that chemical variations on a microscopic scale also exist in deep-sea ferromanganese concretions.

Winterhalter and Siivola performed the first detailed study of the internal structure of ferromanganese concretions from the Baltic Sea.[4] They noted a close correlation between P and the Fe-rich layers in the concretions. Suess and Djafari[5] noted that the outer layers of concretions from Kiel Bay in the Baltic Sea contained anomalously high concentrations of Zn, Pb, Cd and Cu. They concluded that this was an effect of increased anthropogenic input of these elements. However, Ingri and Pontér[6] showed that even elements with no known pollution source, *e.g.* Y and La, show enrichment in surface layers in ferromanganese concretions from the Gulf of Bothnia. There exist natural enrichment processes, largely governed by the redox level, which make it difficult to distinguish between natural and man-made contributions of trace metals in concretions.[6] However, further work in the Kiel Bay[7] suggests that concretions in this area reflect pollution effects and it has been proposed that laser ablation-inductively coupled plasma-mass spectrometry (LA-ICP-MS) could be a useful method to monitor the changes in trace metal incorporation in the concretions.

Recently a growth rate estimate on ferromanganese concretions from the Baltic Sea has been performed, by using $^{226}Ra_{excess}$/Ba ratios in individual layers of the nodules.[8] It was concluded that it is not yet clear whether ferromanganese concretions can be used as an archive for postglacial variations in Baltic water masses. More data using Nd-, Sr- and Pb-isotope systematics on $^{226}Ra_{excess}$/Ba dated ferromanganese concretions are needed. Beside these isotope systems, detailed measurements of individual element distributions in the interior of concretions are of utmost importance in order to understand concretion formation and hence evaluate their potential in, *e.g.* pollution studies.

Based on the acid digestion procedure described previously,[9] it is possible to gain quantitative information on the concentrations of about 60 elements using low mg or even sub-mg amounts of material. However, our experience with the micro-sampling of concretions has shown that the lowest amount of material that can be reliably sampled is in the range of 0.5–0.7 mg. For smaller samples, errors associated with collection and weighing, as well as contamination risks, preclude accurate analyses. As a result, the lowest three-dimensional resolution is on the order of 0.7 mm^3, providing about 20–25 sub-samples over the cross-section of a concretion, 20 mm in diameter. As a rule, the growth structure of concretions is in the few μm range, thus only averaged information from many structural segments can be obtained, resulting in only modest spatial information gain compared to whole concretion analysis. Moreover, at least two working days are required for complete sampling, digestion and analysis of one concretion (two cross-sections, 40–50 sub-samples).

The spatial resolution in the analysis of solid samples can be greatly improved by using LA, and successful applications of this technique for assessing element distributions on the sub-mm scale in a variety of matrices, such as tree rings,[10–17]

† Presented at the 2002 Winter Conference on Plasma Spectrochemistry, Scottsdale, AZ, January 6–10, 2002.

 DOI: 10.1039/b204262m

corals,[18,19] mussel shells,[20,21] fish otoliths,[19,22,23] teeth,[24–26] *etc.*, have been reported. Alongside significant time savings (due to the limited sample preparation as well as the absence of uptake and washing times that are inevitable using traditional solution nebulisation), LA offers the additional advantage of reduced spectral interferences caused by oxide and hydroxide species[27,28] (due to the absence of solvent at dry plasma conditions). However, quantification by using LA-ICP-MS is much more complicated than for solution nebulisation.[29] An additional challenge is correction for possible variations in ablation efficiency, which may be caused by a variety of difficult to control parameters[27,29] including: aging of the laser flashlamp; sample positioning inside the ablation chamber or changing the position of the sampling area relative to the Ar flow during raster ablation; spatial inhomogeneities in the structure, density or colour of the material under investigation. In samples with a finely laminated structure, *e.g.* shallow-sea concretions,[30] the latter may, if not corrected adequately, result in false distribution patterns.

In this paper, a multielement procedure for high spatial resolution analysis of ferromanganese concretions using LA-ICP-MS is described, with emphasis on the optimisation of measuring parameters, internal standard correction and quantification by external calibration against matrix-matched standards.

Experimental

Instrumentation

The ICP-sector field MS (ICP-MS) instrument used was the ELEMENT, equipped with both a standard solution nebulisation introduction system (SN) and a LA UV LaserProbe unit (both from Finnigan MAT, Bremen, Germany). In this work, only two resolution modes – low ($m/\Delta m$ about 300) and medium ($m/\Delta m \approx 4500$) – have been used. Details on the instrumental operating conditions are reported in Table 1. Measuring parameters were, in general, the same as those used in a previous study,[9] with the following modifications:

Isotopes of Rh, Pd, Ru, Ir, Os, Re, Ge and Au have not been included, as these elements are typically present in ferromanganese concretions from the Gulf of Bothnia at sub-ng g^{-1} concentrations;

The acquisition window in low resolution mode was reduced to 10% (instead of 50% for SN) while keeping the number of samples per nuclide constant;

Only one scan per resolution was used (instead of 15 for SN).

Due to these modifications, the measuring time per sample was decreased from a few minutes to less than 24 s.

Sample preparation and standards

Ferromanganese concretions used in this study were collected from the Gulf of Bothnia, northern Baltic Sea. A ferromanganese nodule reference material, Nod-P1 (Branch of Geochemistry, U.S. Geological Survey, 923 National Center, Reston, Virginia 22092, USA), was also employed.

It is known that element concentrations in concretions are governed by the relative proportions of three major phases: aluminosilicates, Fe-oxyhydroxides and Mn-oxyhydroxides.[31–33] Additionally, sampling location and concretion size may be of importance. As successful external calibration requires a set of standards with varying concentrations of the elements under investigation, concretions have been separated in different groups by colour, structure, size and sampling location. Pieces of the concretions used for the preparation of matrix-matched standards were first dried at 50 °C to constant mass, then ground using an iron grinder (slightly modified steel grinder from Lun-Mek AB, Mariehamn, Åland), followed by sieving through a 62 μm plastic sieve. At least 5 g of each material was prepared. Between each sample processed, all equipment was carefully cleaned (quartz sand grinding followed by wiping with ethanol-moisturized tissue paper for the grinder, and washing with ethanol followed by compressed air hosing for the sieve) in order to reduce cross-contamination. These ferromanganese concentrates were analysed by ICP-MS following acid digestion in accordance with the analytical procedure reported previously.[9] Based on the results thus obtained, six concentrate samples were selected, providing the widest possible concentration ranges for the elements studied. Finally, a set of seven matrix-matched standards for LA was prepared by pressing about 200 mg of the selected concentrates, as well as Nod P1 reference material, into 12 mm tablets, using a conventional stainless steel press (Herzog TP20, (Osnabruck, Germany) at a total thrust of 10 tons applied for 2 min. In order to reduce Cr and Ni contamination, it is important to use Teflon spacers to separate the press tool surfaces from the concretion tablet. However, the concretion powder tends to get pressed into the Teflon, thus making separation of the spacers from the tablet difficult. Occasionally, this causes marring of the tablet surface and the need to prepare more than one tablet from each separate in order to obtain satisfactory results.

Table 1 LA-ICP-MS operating conditions with optimum parameters given in parentheses

Rf power/W	1100–1500 (1300)
Argon gas flow rates/l min^{-1}	
Coolant	15.3
Auxiliary	1.00
Nebuliser	0.6–1.6 (LA 1.25, SN 0.90)
Ion sampling depth/mm	9
Ion lens settings	Adjusted to obtain maximum signal intensity
Torch	Fassel 1.5mm i.d. Injector
Nebuliser	Micromist, Glass Expansion, Romainmotier, Switzerland
Spray chamber	Scott type PFE (double-pass)
Sample cone	Nickel, 1.1 mm orifice diameter
Skimmer	Nickel, 0.8 mm orifice diameter
Laser (Nd:YAG)	
Wavelength/nm	266
Pulse width/ns	3
Pulse energy/mJ	0.1–3.0 (1.0)
Ablation diameter/μm	5–50 (20)
Distance between points/μm	30–50 (30)
Repetition rate/Hz	1–20 (8)
Number of shots per point	1–99 (20)
Sample scan mode	Line or raster scan across (line for standard, raster for concretion analysis)
Time delay/s	0.1

For the preparation of sample used for high spatial resolution analysis, the concretions were cut in half by a diamond wafering blade cutter (102 × 0.3 × 12.7 mm; Buehler, LTD., USA). The cutter was an Isomet™, low speed saw (Buehler, Evanstone, USA). Unfortunately, the blade contaminates the sample surface with Cu and Sn, which is difficult to prevent or remove. Consequently, the accurate determination of these elements by LA will require pre-ablation of the concretion surface before the actual analysis.

In order to test the performance of the quantification approach used in this study, micro-samples were taken along the major axis from one half of one of the largest concretions (about 25 mm), prior to acid dissolution and quantitative analysis by SN-ICP-MS,[9] while the second half was used for LA.

Optimisation of ICP parameters

Though it is well known that careful optimisation of plasma parameters is of primary importance in order to produce a stable and high signal for analytes of interest, as well as to reduce possible matrix effects,[34] the number of LA-ICP-MS

studies dealing with this issue is very limited. In this work, the effects of variable carrier gas flow rates (FRs) and forward power (rf power) settings on analyte signal intensities were studied while continuously ablating a tablet pressed from the nodule reference material. Such parameters as sampling depth and torch injector diameter have been kept constant throughout the experiments. It was shown[35] that using ICP-MS with SN, the intensity maxima appear at nearly the same FR for all elements, independently of both atomic mass and ionisation potential (IP). For the particular ICP-SFMS instrument used in this study, the optimum nebuliser gas FR was about 0.75 l min^{-1} when operating at an rf power of 1350 W with the SN introduction system.

With LA, the dependence of analyte signals on carrier gas FR is far more complicated (Fig. 1). At 1100 W rf power, Fe and Mn intensities recorded at different FRs exhibit two maxima at 0.86 l min^{-1} and at 1.15 l min^{-1}. There are only minor differences in intensities monitored at these FRs, though as a rule, slightly higher sensitivities were recorded at the second maximum. Similar behaviour was found for the largest of three groups of elements tested. For As and B (as well as for Be, Br, Cd, I, P, Sb, Se, Te and Zn), a single maximum at 1.15 l min^{-1} is apparent. For Th and Zr (as well as Y, Sc, rare earth elements, Hf, W and Ta), the highest intensities were obtained at 0.86 l min^{-1} with about a two-fold drop in signal at 1.15 l min^{-1}. For the latter group of elements, significant increases in oxide formation were found at FRs higher than 1.10 l min^{-1}. Only modest sensitivity gains can be obtained by increasing the rf power from 1100 W to 1300 W. The pattern of FR plots is almost the same, with slight shifts in the positions of the response maxima towards higher FRs. In contrast, further increase in the rf power to 1500 W results in significant losses of intensity, which are particularly severe for elements with high first IP, as well as in notable changes in optimum FRs. The FR distribution now has only one maximum at about 1.30 l min^{-1} for elements of the second group (*e.g.* As and B in Fig. 1) and at about 1.05–1.10 l min^{-1} for the rest of the elements. The use of such high rf power settings is impractical as it significantly increases Si blanks and could potentially result in rapid destruction of the plasma torch by overheating.

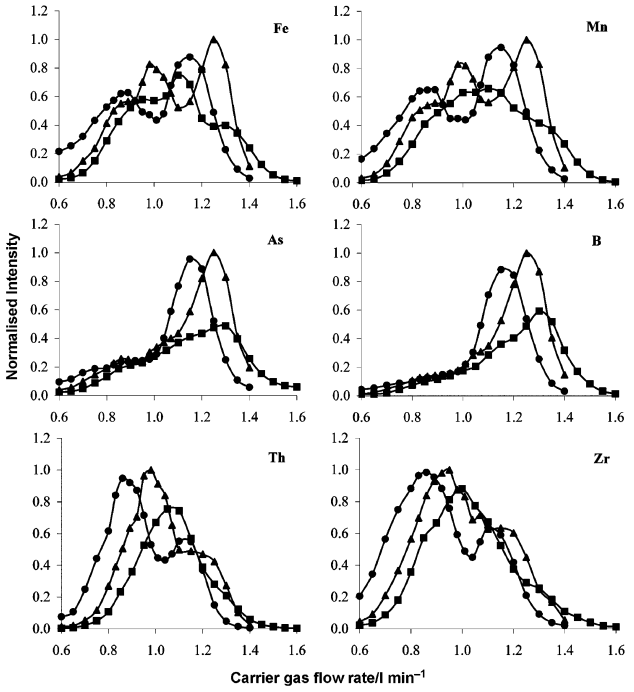

Fig. 1 Optimisation of carrier gas flow rate for pairs of analytes representing the behaviour of three element groups in LA-ICP-MS, at rf power settings of 1100 W (circles), 1300 W (triangles) and 1500 W (squares).

The reason why the intensities for different groups of analytes peak at different FRs while using 'dry' plasma conditions is not clear at the moment, and investigation of the exact nature of the processes involved was beyond the scope of this study. However, it is obvious that the use of compromise ICP operating conditions is inevitable for LA-ICP-MS. The first element group considered (Fe, Mn, *etc.*) will exhibit relatively uniform response in the FR range from 0.9 to 1.3 l min^{-1}, elements with high first IP (As, B, *etc.*) would require 1.15–1.25 l min^{-1}, while FR settings in the range 0.85–0.95 l min^{-1} are optimal for refractory elements (Th, Zr, *etc.*). For the subsequent experiments, the rf power was set to 1300 W and the carrier gas FR was adjusted to maximise the Fe and Mn signals. This provides optimum conditions for all but the refractory elements. Needless to say, due to the use of the significantly higher FR (about 1.25 l min^{-1}) compared to SN operation, ion lens settings (extraction lens in particular) have to be re-adjusted for LA sampling. The compromised optimum FRs used during the following experiments for LA and SN-ICP-MS analysis were 1.25 and 0.90 l min^{-1} respectively.

It is important to note that optimal ICP parameters proved to be relatively independent of LA parameters. For example, it was found that a three-fold increase in ablation energy affects the signal intensities for all elements tested, but does not change the pattern of the FR plots illustrated in Fig. 1. Hence, optimisation of ICP and LA parameters can be performed separately.

Optimisation of LA parameters

Optimisation of laser parameters was performed while line ablating a pressed tablet of the Nod-P1 reference material, recording two sets of data (20 measurements each) for each change made. In order to investigate possible effects originating from differences in the position of the sampling site inside the ablation chamber on the response, the first set was acquired while ablating parallel, and the second perpendicular, to the Ar flow through the chamber. As a rule, differences between the mean intensities for these two data sets were statistically insignificant (*t*-test; $P < 0.05$). Apparently, differences in the orientation of the ablation line relative to the carrier gas flow have no major impact on analyte transport (at least within a single tablet) and thereby, only results from the first set will be presented. ICP operating conditions were fixed during these experiments. The parameters investigated were: pulse repetition rate, number of shots per point, ablation energy and spot diameter. Each parameter was optimised regarding analyte signal intensities and noise levels, calculated as relative standard deviations (RSDs) for 20 measurements. Fig. 2 summarises the regularities revealed for selected analytes.

It was found (Fig. 2a) that analyte intensities increase with pulse frequency from 1 to 12 Hz. For this experiment, the laser was programmed to perform only one shot per ablation point. Further increases in repetition rate up to 20 Hz (highest available setting for the current LA system) have little affect on the signal intensity. The best signal stabilities were obtained with repetition rates in the range 8–12 Hz. Increasing the number of shots per point from 1 to 10 while keeping the repetition rate at 8 Hz resulted in no, or only moderate, losses of sensitivity (Fig. 2b), though the signal intensities dropped by as much as 80% at higher numbers of shots. This parameter does not notably affect signal stability. There is an almost linear relationship between signal intensity and laser energy in the range from 0.1 and 3 mJ (Fig. 2c) that provides a useful means to regulate the combined sensitivity of LA-ICP-MS. However, there is an almost two-fold increase in RSD at energies above 1 mJ. The final parameter tested was ablation spot diameter (from 5 to 50 μm) and it was found to have no

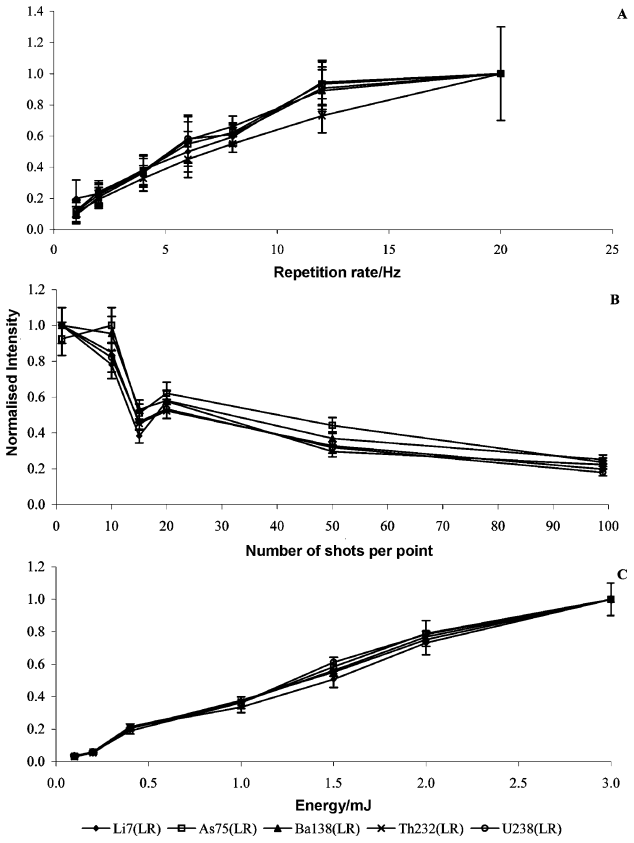

Fig. 2 Optimisation of (a) repetition rate, (b) number of shots per point and (c) laser energy. During each set of experiments, the remaining parameters were held constant at the optimum values given in Table 1.

significant effect on intensities for the elements evaluated (results not shown). Signal stabilities, on the other hand, slightly deteriorated at ablation diameters below 20 μm.

From the requirement of high sensitivity, LA should be performed using high energies and repetition rates, while keeping the number of shorts per point at a minimum. However, in order to maintain high signal stability and spatial resolution, the following LA parameters were chosen: 1 mJ energy, 20 ablation shots per point at 8 Hz repetition rate, 20 μm ablation diameter with distance between ablation points of 30 μm. Additionally, to meet the requirements of high spatial resolution, especially when analysing real concretions, the laser was programmed to ablate along a line perpendicular to the measurement axis at each sampling point, *i.e.*, at each layer in the concretion, using the optimised LA sampling parameters. This ensures that representative data are acquired for a single layer in the concretion structure, while maintaining a constant supply of ablated material for the entire duration of a complete ICP-SFMS measurement cycle (24 s, including measurements in both low and medium resolution mode).

Detection limits

Detection limits for LA sample introduction were computed as three times the standard deviation for the carrier gas blank divided by the slope of the calibration line established using seven pressed concretion tablets. It is important to note, that the LA-ICP-SFMS sensitivity factors used for these calculations were obtained using the optimised LA parameters, in particular 1 mJ laser energy. As gas blanks are independent of laser energy, the detection limits can be lowered significantly by using higher energy, as suggested by the results given in Fig. 2c. For comparative purposes, the detection limits obtained for acid digested concretions analysed by conventional SN-ICP-SFMS are used.[9] These were defined as three times the standard deviation for 11 sample preparation blanks, assuming a final dilution factor of 5×10^4.

Results and discussion

Internal standardisation

Internal standards are widely applied in the analysis of solutions by ICP-based techniques. On the other hand, in applications of LA for the direct analysis of solid samples, addition of an internal standard is complicated and a matrix element is often selected instead.[36–40] This requires prior knowledge of the candidate internal standards' concentration in the sample and calibration materials. To this end, Si has been used as an internal standard for glass analysis[38] and Ca for seashells, corals, otoliths[18–23] and fluid inclusions.[41] Regarding ferromanganese concretions, both Fe and Mn could be considered viable candidates, but the relative concentrations of these elements vary both between, and within, concretions. However, extensive analyses of concretion samples and reference materials, using a previously developed digestion method,[9] have shown that the sum of the Fe and Mn concentrations is relatively constant at 32.9 ± 3.3% ($n = 65$ samples). For this reason, the sum of the measured intensities for Fe and Mn may serve the purposes of internal standardisation.

The response of the ICP-MS instrument to each of the monitored ions, $^{56}Fe^+$ and $^{55}Mn^+$, is not identical due to differences in relative isotopic abundances,[42] IP[43] and mass discrimination effects.[44] These effects are combined in a relative response correction factor, k (dimensionless), used to calculate the combined internal standard count rate, I_{cis} (counts s^{-1}), as

$$I_{cis} = k\, I_{Fe} + I_{Mn}$$

where I_{Fe} and I_{Mn} are the measured count rates for $^{56}Fe^+$ and $^{55}Mn^+$, respectively. The correction factor has been empirically determined to be $k = 1.25 \pm 0.05$ for both LA and SN with the instrumentation used in the current study.

Application of internal standardisation to LA is particularly important for samples exhibiting pronounced spatial variations in composition, as is the case for concretions. Although the sum of the Fe and Mn concentrations is fairly constant, as mentioned above, each of these elements is unevenly distributed through layers of varying composition, colour and density in the concretion material. Consequently, the intensities fluctuate when ablating the sample as a result of variations in concentrations and in laser energy coupling to the surface.[45] To account for these variations, the intensity for any element generated by LA at a given position, $I_{X,p}$, is simply normalised to the combined internal standard count rate at an arbitrary starting point, $^0I_{cis}$

$$^{norm}I_{X,p} = I_{X,p}(^0I_{cis}/I_{cis,p})$$

Normalisation in this manner allows more faithful spatial mapping of elemental compositions than otherwise. One caveat is that the sample should not contain major inclusions of other materials, such as ingrown sediment particles, as this could result in extensive overestimation of $^{norm}I_{X,p}$. This problem would, however, be immediately evident in the normalised data for other elements characteristic of sediment particles, such as Al, Ca and Si.

External calibration

Calibration standard tablets were placed in the ablation cell together with the concretion sample to be analysed. The design of the ablation chamber allows accommodation of up to seven tablets plus one concretion with a diameter of 20–25 mm (or 2–3 concretions with diameters below 10 mm). Hence, the entire measuring sequence can be performed without opening the

chamber. The sequence started with the analysis of the carrier gas with the laser switched off (Ar blank). The laser was then programmed to perform line ablation across each of the tablets parallel to the carrier gas flow. Analysis time per tablet was about 4 min, thus allowing 10 separate measurements to be acquired. All raw intensity data were first blank subtracted using mean gas blank values, followed by internal standard correction in accordance with the procedure described in the previous section. The mean of blank subtracted and internal standard corrected intensities for each tablet, together with concentrations determined on the sub-sample of tablet material were used to determine LA-ICP-MS sensitivity coefficients for each isotope using linear regression analysis. In Table 2 the correlation coefficients (R^2), slopes of the calibration graphs and ranges of element concentrations are presented. For most elements, R^2 is close to 1 but there are exceptions (Pt, V, Si, Na and Al) for which $R^2 < 0.7$. In most cases, this is caused by the narrow concentration distribution centred far from the origin of the calibration line. For Pt, it is mainly due to the low concentration levels seen in the materials, resulting in larger uncertainties in the data and thereby poorer accuracy.

Obviously, R^2 values for LA can never be expected to be on a par with those achieved using SN-ICP-MS. The fact that calibration points produced by using tablets pressed from concentrates with very different Fe and Mn concentrations (and therefore different colours and structures) give nearly perfect calibration lines for the majority of tested elements, clearly demonstrates the efficacy of the internal standardisation procedure used. For applications in which absolute accuracy and highest precision are not the primary goals, then the calibration strategy described here could be considerably simplified by reducing the number of calibrants employed.

By comparing the slopes of calibration graphs obtained by LA (Table 2) and SN using the same ICP-MS instrument, an interesting observation can be made. Fig. 3 shows SN/LA sensitivity (S) ratios, for a suite of analytes. These ratios are normalised to average sensitivity for SN and LA for the elements Mn and Fe (S_{Fe+Mn}) (elements used in the combined internal standard). It is obvious that LA produces higher relative sensitivities for low-mass elements (Li and Be), as well as for elements with high first IPs (P, S, As, Br, Sb, Te, and I). The opposite is true for Al Si, Ca, Sc, Y, Zr, rare earth elements, Hf, Ta and Th. These differences in relative sensitivities between the two modes of sample introduction are likely caused by a combination of various processes occurring during ablation, sample transport and in the ICP, as well as during ion extraction and transport through the mass spectrometer. One of the possible mechanisms is incomplete dissociation of large particles entering the ICP, which would discriminate against refractory elements. In order to check the occurrence of such process, calibration of the LA-ICP-MS system was performed in a similar fashion to that described above while filtering out the largest particles produced during ablation by means of a mineral wool plug (approximately 200 mg) inserted in the line (0.8 cm inner diameter) connecting the ablation chamber with the ICP resulting in a 3–4 cm plug.[46] Although filtration resulted in an approximately three-fold decrease in response, this drop was similar for all elements, providing an unchanged pattern of normalised LA to SN sensitivities (Fig. 3). These results suggests that there are no apparent differences in the composition of small and large particles produced by LA, as well as that incomplete dissociation (if such takes place) weakly depends on particle size.

By comparing FR dependence plots for different groups of elements (Fig. 1), it is obvious that the differences in relative sensitivities between LA and SN (at least partly) can be explained by differences in analyte distributions in the ICP. By using lower carrier gas FRs than the one optimal for the sum of Fe and Mn intensities, it is possible improve sensitivities for refractory elements at the expense of other analytes, especially ones with high IPs. Consequently, the magnitude of the differences in relative sensitivities between LA and SN would be greatly reduced.

Regardless of the exact nature of the mechanisms involved, these effects will not impact the accuracy of analytical results produced by external calibration against matrix-matched standards, given that the same carrier gas FR is used for both standards and samples. On the other hand, they may limit the usefulness of alternative quantification strategies, such as dual LA-SN calibration,[47–51] calibration utilising non-matrix matched standards[18–23] or matrix-matched standards spiked with analyte elements[17,52,53] and internal standardisation of LA data relative to the response of major matrix elements prior to quantification using SN sensitivities.[36–40]

Table 2 Correlation coefficients (R^2) and slopes [counts s^{-1} ($\mu g\ g^{-1}$)$^{-1}$] of the calibration functions obtained for linear regression analysis of LA-ICP-MS data for pressed concretion tablets (n = 7). 'Min' and 'max' indicate the range of found concentrations ($\mu g\ g^{-1}$) present in the standards as determined by SN-ICP-MS following acid digestion[9]

Isotope	R^2	Slope	Min	Max
Al27[a]	0.506	28	14600	44000
As75	0.997	1500	65	800
B11	0.873	820	7.8	95
Ba138	0.857	2900	650	4500
Be9	0.969	390	0.58	2.5
Bi209	0.999	6100	0.04	5.8
Cd111	0.986	380	0.09	23
Ce140	0.965	3100	19	300
Co59[a]	0.999	86	50	2300
Cs133	0.958	6000	0.90	4.4
Cu63[a]	1.000	37	9.0	11200
Dy163	0.985	790	1.3	27
Er167	0.987	700	0.71	14
Eu153	0.994	2300	0.30	7.6
Fe56[a]	0.974	92	43600	288000
Ga69[a]	0.952	65	3.8	28
Gd160	0.986	740	1.5	30
Hf180	0.891	830	0.53	4.2
Ho165	0.985	3100	0.26	5.0
I127	0.875	3200	29	100
La139	0.944	2200	10	100
Li7	0.998	1300	8.9	140
Lu175	0.979	3200	0.10	1.8
Mg26[a]	0.922	6.5	7000	20300
Mn55[a]	0.979	115	6400	296000
Mo95	0.994	690	20	760
Na23[a]	0.513	57	9600	17100
Nb93	0.936	2600	2.1	21
Nd146	0.967	580	8.7	130
Ni60[a]	1.000	23	42	13500
P31[a]	0.988	15	1300	35400
Pb208	1.000	3600	3.9	480
Pr141	0.972	3200	2.3	31
Pt194	0.787	1100	<0.04	0.12
Rb85	0.829	3000	27	97
Sb121	1.000	2400	0.24	49
Sc45[a]	0.739	52	2.9	9.7
Si28[a]	0.518	19	46500	103000
Sm147	0.980	540	1.6	31
Sn120	0.775	2500	0.59	1.9
Sr88	0.877	2600	380	800
Tb159	0.992	3100	0.21	4.9
Te125	0.995	370	0.08	4.8
Th232	0.957	2800	2.1	17
Ti47[a]	0.768	4.7	640	2800
Tl205	1.000	5300	0.26	210
Tm169	0.965	3400	0.10	1.9
U238	0.992	6000	2.4	18
V51[a]	0.655	44	38	510
W184	0.999	1200	2.9	58
Y89	0.978	2200	7.2	90
Yb171	0.982	520	0.68	13
Zn64[a]	0.860	22	45	2000
Zr90	0.962	1200	17	280

[a] Measured in medium resolution mode (MRM).

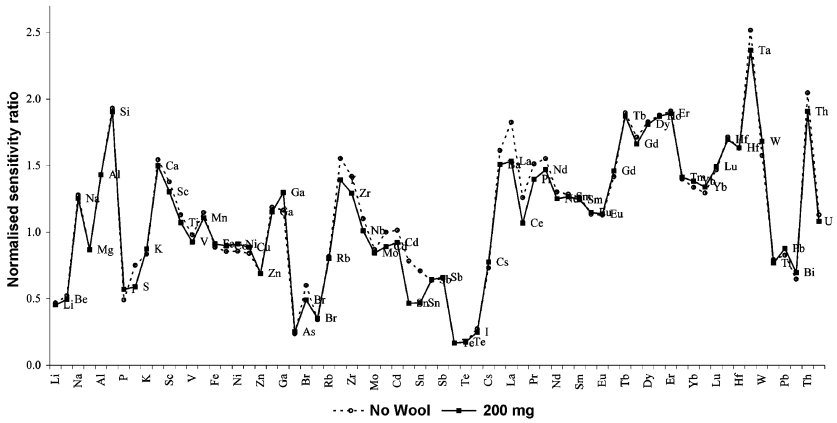

Fig. 3 Normalised sensitivity ratios [= (SX)SN/(SX.)LA*(SMn+Fe)LA/(SMn+Fe)SN] with (filled squares, solid line) and without (open circles, dotted line) insertion of 200 mg mineral wool in the transport line exiting the ablation cell, sample ablated is the Nod-P1 reference material.

In order to evaluate the accuracy of the method, the median concentrations of element distributions across two segments of the same concretion were compared (Fig. 4). One distribution (24 points) was obtained by micro-sampling (sample size below 1 mg) followed by acid digestion and SN-ICP-MS analysis.[9] The other segment was analysed by LA-ICP-MS providing approximately 500 points across the concretion. For the majority of the elements tested, results of these two methods agree to within 20%, with exceptionally good agreement (differences below 10%) for elements determined in low resolution mode (Cd, Sb, rare earth elements, Pb, Tl, Bi, Th, *etc.*). The poorest agreement was found for Cu and Sn, the elements affected by contamination from the cutter that will obviously impair the accuracy of the LA results to the greatest extent.

High spatial resolution concretion analysis

Before providing a few selected examples of the kinds of information contained in a concretion that can be revealed using LA-ICP-MS, it is pertinent to assess the capabilities and limitations inherent in the developed method. Referring to Table 3, the relatively poor detection limits for Mn, Fe and Si are due to elevated blank levels caused by contamination of cones by sample matrix (Mn and Fe) as well as by contributions from the ICP torch (Si). For about 30 elements, slightly better detection limits are achieved using SN-ICP-MS following acid digestion. However, as illustrated in Fig. 4, LA-ICP-MS detection capabilities were adequate for the determination of all tested analytes in shallow sea concretions, in spite of the lower trace element content compared to marine concretions, such as the reference material Nod-P1.

The following examples are based on results obtained for a relatively large spheroidal concretion (25 mm diameter), collected from the Gulf of Bothnia and analysed with a spatial resolution of about 60 μm over the cross-section, thus providing an almost 20-fold improvement in resolution compared to micro-sampling. Analysis of this sample was performed in the same manner as explained above, commencing with external calibration, gas blank measurement, start of the concretion ablation sequence, and a short delay for signal stabilisation before data acquisition. It should be emphasised that the laser was programmed to ablate along a line perpendicular to the measurement axis at each sampling point, *i.e.*, at each layer in the concretion, using the optimised LA sampling parameters. In this way, it was possible to acquire data for all the elements, including measurements in both low and medium resolution mode, without sacrificing spatial resolution.

As expected, given that the combined Fe plus Mn content is fairly constant, both within and between concretions, the individual concentrations of these elements are distinctly anti-correlated in the studied material. Surprisingly though, there is no radial symmetry in the layers, in spite of the fact that measurements were made from one side to the other through the centre of the concretion. (Results for these major elements are not shown here. However, as the same is true for the majority of the elements, the data for Zn reproduced in Fig. 5b serve to exemplify the point.) This asymmetry could be a consequence of two factors. First, the centre of the concretion is not necessarily the centre of growth, and therefore the layers themselves need not be symmetric. The second possibility is that the rates of supply and incorporation of elements in the concretion vary over the surface, because the data reflect conditions towards the upper (facing seawater, although buried in the superficial sediment), and lower (facing the underlying sediment) sides of the concretion.

Mo and Zn are two elements that are positively correlated with the Mn-rich phase in the concretion. However, the scatter about the linear correlation plot with Mn is much greater for

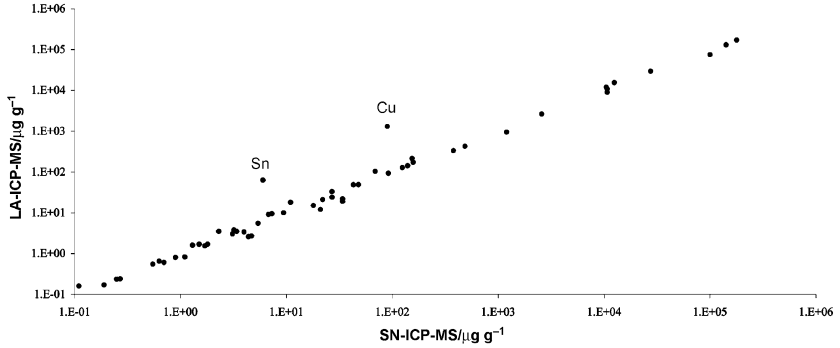

Fig. 4 Comparison of results for all elements, obtained by LA-ICP-MS and SN-ICP-MS for a concretion sample. Discrepancies for Sn and Cu are caused by contamination from the cutter blade.

Table 3 Detection limits (μg g^{-1})

	LA	SN[9]
Al	8	4
As	0.26	1
B	0.24	10
Ba	0.10	0.10
Be	0.06	0.07
Bi	0.02	0.005
Cd	0.10	0.05
Ce	0.02	0.06
Co	0.08	0.10
Cs	0.04	0.008
Cu	2	4
Dy	0.01	0.001
Er	0.02	0.0005
Eu	0.02	0.002
Fe	18	2
Ga	0.07	0.02
Gd	0.04	0.002
Hf	0.001	0.001
Ho	0.01	0.0004
I	1	0.50
La	0.03	0.03
Li	1	1
Lu	0.01	0.0009
Mg	6	4
Mn	1	0.6
Mo	0.07	0.2
Na	60	300
Nb	0.04	0.008
Nd	0.09	0.02
Ni	2	2
P	3	4
Pb	0.10	0.3
Pr	0.04	0.003
Pt	0.04	0.002
Rb	0.26	0.20
Sb	0.02	0.04
Sc	0.02	0.20
Si	300	100
Sm	0.02	0.002
Sn	0.11	0.20
Sr	0.06	0.20
Tb	0.01	0.0006
Te	0.09	0.025
Th	0.0004	0.004
Ti	1	1
Tl	0.03	0.007
Tm	0.01	0.0008
U	0.0002	0.004
V	0.32	0.07
W	0.001	0.05
Y	0.03	0.02
Yb	0.02	0.002
Zn	3	2
Zr	0.03	0.03

Zn ($R^2 = 0.30$) compared with Mo ($R^2 = 0.70$). Concentration ratios between Mo and Zn reveal a clear pattern, with three-fold lower ratios towards the left-hand side of Fig. 5a. The concentration of Mn is similar in all the Mn-rich layers and cannot explain the differences in incorporation between Mo and Zn. As the Mo and Mn concentrations are highly linearly correlated, and because other environmental factors have little effect on the Mo/Mn ratio.[6]

Zn is possibly influenced by the *in-situ* redox conditions in the sediment, as discussed in detail elsewhere.[6] The magnitude of the Ce-anomaly in ferromanganese concretions reflects the redox level of the environment of deposition.[54,55] This anomaly is defined as

$$Ce_{anomaly} = \frac{Ce_{norm}}{(2/3La_{norm} + 1/3Nd_{norm})}$$

where the element symbols represent concentrations in the concretion normalised to values for a standard reference sample.

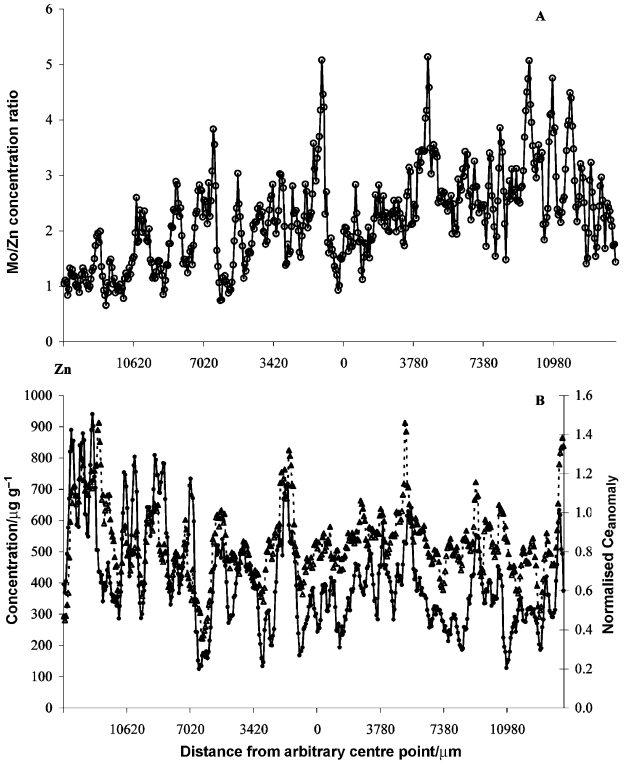

Fig. 5 Examples of high spatial resolution data obtained for a concretion cross-section by LA-ICP-MS: (a) ratio between Mo and Zn concentrations in μg g^{-1}; (b) Zn concentrations (circles, solid line) and corresponding Ce-anomaly values (triangles, dotted line).

Data from the Gulf of Bothnia showed that the Ce-anomaly in spherical concretions, buried in a 6 cm thick oxidised surface sediment, increased towards the sediment–water interface,[56] thus indicating an increased *in-situ* redox level.

The method described here makes it relatively simple to compare trace element concentrations (in relation to tedious sub sampling of layers within a concretion) between different Mn–Fe layers within one concretion and also to compare concentration values with other concretions and areas. It is also possible to calculate the *in-situ* Ce-anomaly with high spatial resolution within a single concretion. Data for the Ce-anomaly in Fig. 5b, indicate that different Mn-rich layers were formed under slightly different redox conditions. There is a positive correlation between high Zn concentrations and an increased Ce-anomaly. Hence, the relative enrichment of Zn could partly be related to an increased redox level at the time of deposition. This has important implications for the use of concretions as historical pollution records.

Conclusions

Variations in relative instrumental sensitivity between elements, commonly termed "fractionation" in the LA-ICP-MS literature,[46] might not be entirely attributable to the preferential ablation of more volatile analytes, but rather due to differences in the shapes of the flow rate dependent response curves for different analytes (see Fig. 1). Further evidence for this hypothesis is provided by the fact that inserting a mineral wool filter after the ablation chamber did not affect the shape of the normalised intensity plot shown in Fig. 3. This demonstrates that LA of the concretion samples generates particles of uniform chemical composition, at least to the, albeit limited, resolution of this experiment.

Use of a combined internal standard, consisting of the weighted sum of intensities for Fe and Mn, provides an effective component of the proposed calibration strategy for

the direct analysis of ferromanganese concretions by LA-ICP-MS. Although this novel approach is based on the somewhat fortuitous constancy of the sum of Fe and Mn concentrations (32.9 $\pm$ 3.3%) in this particular type of sample, extension to other materials would appear to be quite feasible.

The second component of the calibration strategy is the preparation of pressed tablets from ground concretion samples, including the reference material Nod-P1. By exploiting the inherent variations in composition available in ferromanganese concretions, the use of these matrix-matched, multi-level calibration standards confirmed the linearity of the instrumental response and the accuracy of the method over the concentration ranges typically encountered in natural samples. This enables quantitative measurements of elements and elemental ratios with μm-scale resolution, *in-situ*, in ferromanganese concretions.

For the elucidation of the prevailing environmental conditions during concretion formation, the ability to obtain accurate analytical data with μm-scale resolution is decisive. As an example, redox conditions can be inferred from the magnitude of the Ce-anomaly at any given point in a concretion (Fig. 5b). This requires reliable concentration data for no less than three different trace analytes (Ce, La and Nd), in addition to the internal standard elements, which are major constituents. The LA-ICP-MS method presented here fulfils these requirements, and will facilitate interpretation of changes in element supply and incorporation, as well as the comparison between different regions *via* concretion analyses. Quantitative measurements of element ratios should also provide a useful tool for studying regional environmental changes reflected in the composition of ferromanganese concretions.

Acknowledgements

Special thanks are due Mr. Erik Burman, SGAB Analytica, for valuable help during sample and concretion standard preparation. This study was partly financed by Norrbottens forskningsråd and by the EU's structural fund for Objective 1 Norra Norrland.

References

1 E. N. Cameron, *Ore Microscopy*, Wiley, New York, NY, 1961.
2 G. Arrhenius, Pelagic sediments, in *The Sea*, vol. 3, ed. M. N. Hill, Interscience, New York, 1963, pp. 655–727.
3 R. G. Burns and D. W. Fuerstenau, *Am. Miner.*, 1966, **51**, 895–902.
4 B. Winterhalter and J. Siivola, *C. R. Soc. Geol. Finl.*, 1967, **39**, 161–172.
5 E. Suess and D. Djafari, *Earth Planet. Sci. Lett.*, 1977, **35**, 49–54.
6 J. Ingri and C. Pontér, *Rapp. P.-V. Reun. Cons. Int. Explor. Mer.*, 1986, **186**, 234–243.
7 G. P. Glasby, E. M. Emelyanov, V. A. Zhamoida, G. N. Baturin, T. Leipe, T. Bahlo and P. Bonacker, in *Manganese Mineralization: Geochemistry and Mineralogy of Terrestrial and Marine Deposits*, Geological Society Special Publication, 1997, Special Publication 119, pp. 213–237.
8 V. Liebetrau, A. Eisenhauer, N. Gussone, G. Worner, B. T. Hansen and T. Leipe, *Geochim. Cosmochim. Acta*, 2002, **66**, 73–83.
9 M. D. Axelsson, I. Rodushkin, J. Ingri and B. Öhlander, *Analyst*, 2002, **127**, 76–82.
10 U. Narewski, G. Werner, H. Schultz and C. Vogt, *Fresenius' J. Anal. Chem.*, 2000, **366**, 167–170.
11 T. Prohaska, C. Stadlbauer, R. Wimmer, G. Stingeder, C. Latkoczy, E. Hoffmann and H. Stephanowitz, *Sci. Total Environ.*, 1998, **219**, 29–39.
12 S. A. Wathmough, T. C. Hutchinson and R. D. Evans, *Environ. Sci. Technol.*, 1998, **32**, 2185–2190.
13 S. A. Watmough, T. C. Hutchinson and R. D. Evans, *J. Environ. Qual.*, 1998, **27**, 1087–1094.
14 E. Hoffman, C. Lüdke and H. Stephanowitz, *Fresenius' J. Anal. Chem.*, 1996, **355**, 900–903.
15 C. D. Garbe-Schönberg, C. Reimann and V. A. Pavlov, *Environ. Geol.*, 1997, **32**, 9–16.
16 S. A. Watmough, T. C. Hutchinson and R. D. Evans, *Environ. Sci. Technol.*, 1997, **31**, 114–118.
17 E. Hoffman, C. Lüdke, H. Scholtze and H. Stephanowitz, *Fresenius' J. Anal. Chem.*, 1994, **350**, 253–259.
18 D. J. Sinclair, L. P. J. Kinsley and M. T. McCulloch, *Geochim. Cosmochim. Acta*, 1998, **62**, 1889–1901.
19 S. R. Thorrold and S. Shuttleworth, *Can. J. Fish. Aquat. Sci.*, 2000, **57**, 1232–1242.
20 A. Raith, W. T. Perkins and N. J. G. Pearce, *Fresenius' J. Anal. Chem.*, 1996, **355**, 789–792.
21 V. R. Bellotto and N. Miekeley, *Fresenius' J. Anal. Chem.*, 2000, **367**, 635–640.
22 P. J. Gemperline, R. A. Rulifison and L. Paramore, *Chemometr. Intell. Lab. Syst.*, 2002, **60**, 135–146.
23 D. A. Milton and S. R. Chenery, *Mar. Ecol. Prog. Ser.*, 2001, **222**, 239–251.
24 F. Lochner, J. Appleton, F. Keenan and M. Cooke, *Anal. Chem. Acta*, 1999, **401**, 299–306.
25 A. M. Ghazi, S. Shuttleworth, S. J. Angulo and D. H. Pashley, *J. Anal. At. Spectrom.*, 2000, **15**, 1335–1341.
26 K. M. Lee, J. Appleton, M. Cooke, F. Keenan and K. Saqicka-Kapusta, *Anal. Chim. Acta*, 1999, **395**, 179–185.
27 H. P. Longerich, in *Laser-Ablation-ICPMS in the Earth Sciences*, ed. P. Sylvester, Mineralogical Association of Canada, Ottawa, Ontario, 2001, ch. 2.
28 I. Rodushkin, M. D. Axelsson and E. Burman, *Talanta*, 2000, **51**, 743–759.
29 R. E. Russo, X. L. Mao and O. V. Borisov, *Trends Anal. Chem.*, 1998, **17**, 461–469.
30 C. D. Garbe-Schönberg and G. M. McMurty, *Fresenius' J. Anal. Chem.*, 1994, **350**, 264–271.
31 S. E. Calvert, N. B. Price, G. R. Heath and T. C. Moore, *J. Mar. Res.*, 1978, **36**, 161–183.
32 J. L. Bischoff, D. Z. Piper and K. Leong, *Geochim. Cosmochim. Acta*, 1981, **45**, 2047–2063.
33 Y. H. Li, *Geochim. Cosmochim. Acta*, 1982, **46**, 1053–1060.
34 I. Rodushkin, T. Ruth and D. Klockare, *J. Anal. At. Spectrom.*, 1998, **13**, 159–166.
35 L. Moens, F. Vanhaecke, J. Riondato and R. Dams, *J. Anal. At. Spectrom.*, 1995, **10**, 569–574.
36 A. M. Leach and G. M. Hieftje, *Anal. Chem.*, 2001, **73**, 2959–2967.
37 P. J. Sylvester and S. M. Eggins, *Geostand. Newsl.*, 1997, **21**, 215–229.
38 S. Rings, R. Sievers and M. Jansen, *Fresenius' J. Anal. Chem.*, 1999, **363**, 165–173.
39 P. M. Outridge, W. Doherty and D. C. Gregoire, *J. Geochem. Explor.*, 1998, **60**, 229–240.
40 A. J. Campbell and M. Humayun, *Anal. Chem.*, 1999, **71**, 939–946.
41 A. Moissette, T. J. Shepherd and S. R. Chenery, *J. Anal. At. Spectrom.*, 1996, **11**, 177–185.
42 K. J. R. Rosman and P. D. P. Taylor, *Pure Appl. Chem.*, 1998, **70**, 217–236.
43 *Handbook of Chemistry and Physics*, ed. D. R. Lide, CRC Press, New York, 79th edn., 1998–1999, 10-175-10-176.
44 K. G. Heumann, S. M. Gallus, G. Rädlinger and J. Vogl, *J. Anal. At. Spectrom.*, 1998, **13**, 1001–1008.
45 F. Boue-Bigne, B. J. Masters, J. S. Crighton and B. L. Sharp, *J. Anal. At. Spectrom.*, 1999, **14**, 1665–1672.
46 D. Günther and B. Hattendorf, in *Laser-Ablation-ICPMS in the Earth Sciences*, ed. P. Sylvester, Mineralogical Association of Canada, Ottawa, Ontario, 2001, ch. 6.
47 H. Scholze, H. Stehanowitz, E. Hoffman and J. Skole, *Fresenius' J. Anal. Chem.*, 1994, **350**, 247–252.
48 J. S. Becker, C. Pickardt and H. J. Dietze, *Int. J. Mass Spectrom.*, 2000, **202**, 283–297.
49 C. Pickhardt and J. S. Becker, *Fresenius' J. Anal. Chem.*, 2000, **368**, 173–181.
50 J. S. Becker, C. Pickardt and H.-J. Dietze, *J. Anal. At. Spectrom.*, 2001, **16**, 603–606.
51 D. Günther, H. Cousin, B. Magyar and I. Leopold, *J. Anal. At. Spectrom.*, 1997, **12**, 165–170.
52 C. Pickhardt and J. S. Becker, *Fresenius' J. Anal. Chem.*, 2001, **370**, 534–540.
53 A. Raith and R. C. Hutton, *Fresenius' J. Anal. Chem.*, 1994, **350**, 242–246.
54 G. P. Glasby, *Mar. Chem.*, 1973, **1**, 105–125.
55 D. Z. Piper, *Geochim. Cosmochim. Acta*, 1974, **38**, 1007–1022.
56 J. Ingri and C. Pontér, *Geochim. Cosmochim. Acta*, 1987, **51**, 155–161.